Effects of epitaxial strain on the melting of supported nickel nanoparticles

D. Schebarchov[1] and S. C. Hendy[1,2]

[1]*MacDiarmid Institute for Advanced Materials and Nanotechnology, Industrial Research Ltd., Lower Hutt 5040, New Zealand*

[2]*School of Chemical and Physical Sciences, Victoria University of Wellington, Wellington 6140, New Zealand*

(Received 18 July 2010; revised manuscript received 28 July 2011; published 19 August 2011)

We use molecular dynamics to investigate the effects of substrate-induced epitaxial strain on the melting temperature and equilibrium structure of supported metal nanoparticles. Our model system comprises Ni clusters supported on strained graphene. The clusters are modeled using an embedded atom potential, and the nickel-carbon interactions are described by a Lennard-Jones field with one parameter varied to control the substrate binding strength. We find that, after adjusting for curvature effects due to the clusters' free surface, the melting temperature of supported Ni clusters can shift by hundreds of degrees depending on the cluster-substrate epitaxial relationship. The order of magnitude of this effect is shown to be consistent with prior predictions based on thermodynamic modelling. We also find that sufficiently strong substrate binding leads to a solid-solid transition from icosahedral to lamellar-twinned fcc particles, which occurs via a melt-freeze process. These results illustrate how substrate-induced epitaxial strain can be used to control the phase of metal nanoparticles.

DOI: 10.1103/PhysRevB.84.085407 PACS number(s): 61.46.Bc, 64.70.Nd, 64.70.dj, 61.46.Df

I. INTRODUCTION

That surface effects can depress the melting point of small particles has been known for over a century,[1] yet the finer aspects of size-dependent melting continue to generate interest.[2–4] Most activity has focused on metal nanoparticles, largely because of their increasingly many applications in nanoscale science and technology. For example, metal nanoparticles are often used in catalysis[5–7] and assembly of electronic nanodevices,[8,9] and the effectiveness of their performance strongly depends on their phase and surface structure. As more elaborate applications of metal nanoparticles continue to emerge, accurate prediction and control of their size-dependent melting becomes increasingly important.

Many of the existing thermodynamic models for nanoparticle melting assume spherical symmetry,[3] yielding melting temperatures (T_m) that decrease roughly in proportion with the surface-to-volume ratio. In the absence of surface melting effects, the melting point will occur at a temperature where the free energy of the solid particle is equal to that of the liquid. In this case (known as homogeneous melting[1,3]) it can be shown that the melting temperature follows an expression of the form

$$T_m(R) = T_c(1 - \mathcal{C}R^{-1}), \tag{1}$$

where R is the particle radius of curvature (equal to the radius for a free particle), T_c is the bulk melting temperature, and $\mathcal{C}$ is a model-dependent parameter. The dependence on particle curvature (namely, R^{-1}) in (1) is due to the surface-area–to–volume ratio of a sphere, and $\mathcal{C}$ is related to the difference in surface free energy between the solid and molten particles. If one assumes the change in density during melting to be negligible then $\mathcal{C} = 3(\gamma_s - \gamma_l)/(\rho L)$, where γ_s and γ_l are the solid and liquid surface free energies, L is the latent heat, and ρ is the density. Note that $\mathcal{C} > 0$ since $\gamma_s > \gamma_l$ for most materials. Even though the models from which (1) is derived do not consider particles on a substrate, the R^{-1} dependence is found in much of the available experimental[2,10–12] and simulated[13–16] data for supported (as well as free) metal nanoparticles. It has been argued previously that the role of substrates in melting is to merely reduce the curvature of the nanoparticle free surface[13,14] (i.e., R increases), which is why (1) can still apply in the supported case.

In general, however, a solid particle will form a contact angle (θ_s) that is different from that of the liquid (θ_l), as illustrated in Fig. 1, and the corresponding equilibrium curvatures (R_s^{-1} and R_l^{-1}) will not necessarily be the same. It is important to note that R_s^{-1} and R_l^{-1} depend on the surface energies of *both* the free surface *and* the cluster-substrate interface. This has been considered explicitly in a prior thermodynamic model,[17] yielding a melting temperature

$$T_m(R_s, R_l) = T_c\left[1 - \mathcal{C}R_s^{-1} - \mathcal{D}\left(R_s^{-1} - R_l^{-1}\right)\right] \tag{2}$$

that differs from (1) by $\Delta T_m = -T_c\mathcal{D}(R_s^{-1} - R_l^{-1})$ if one sets $R = R_s$. Note that here $\mathcal{C}$ is the same as in (1) and $\mathcal{D} = 3\gamma_l/(\rho L)$. We see that $\Delta T_m = 0$ only when $R_s = R_l = R$, in which case (1) and (2) are equivalent. But if, for instance, the solid phase is favored over the liquid ($R_s > R_l$) on a given substrate, say, due to epitaxial effects, then a discrepancy of $\Delta T_m \sim 100$ K could arise in some cases.[17]

Indeed, some experiments indicate that microscopic features of the particle-substrate interface can favor a particular phase and shift the transition temperature.[18,19] It is also known that epitaxial effects can alter the melting point of confined thin films[20] and nanoparticles embedded in a matrix,[21] and that favorable epitaxy can even lead to superheating. Presumably, if epitaxial alignment can stabilize the solid state in the embedded case, similar behavior should occur in nanoparticles supported on planar surfaces. To the best of our knowledge,

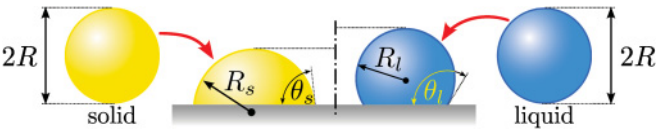

FIG. 1. (Color online) When a particle of fixed volume is placed on a substrate, the resultant contact angle and curvature (of the free surface) will, in general, depend on the phase of the particle.

however, the role and magnitude of epitaxial effects have not yet been assessed in this particular context.

The aim of this study is to show, using molecular dynamics simulations, that favorable epitaxy can significantly raise the melting temperature of metal nanoparticles on planar substrates. Epitaxial strain effects on T_m are isolated and quantified by straining the substrate along the plane, and then adjusting for changes in curvature of the liquid phase. The principle will be demonstrated using Ni clusters supported on graphene. Since nanometer-sized Ni particles are often used as catalysts in carbon nanotube growth,[5–7] the influence of graphene on the melting point of small nickel particles is of interest. More importantly, Ni is a fcc metal with near-neighbor separation of 2.49 Å, closely matching the in-plane lattice constant of graphite (2.46 Å) and yielding excellent epitaxial alignment between the Ni(111) surface and graphene. Furthermore, molten Ni droplets form a contact angle of $\theta_l \sim 50^\circ$ on graphite,[22] leading to a relatively large interfacial area; hence the properties of Ni nanoparticles are likely to be strongly affected by their interaction with a graphitic substrate.

II. COMPUTATIONAL DETAILS

A. Molecular dynamics

All the molecular dynamics simulations reported here were carried out in the canonical ensemble using LAMMPS,[23] with an integration time step of 3 fs (or less in some cases). The temperature of Ni clusters was controlled by a Langevin thermostat (with the time constant set to 1 ps).[24] We used a static graphene sheet as the supporting surface, with the constituent carbon atoms fixed during individual simulations, although in some parts of this study the spacing between substrate carbon atoms was varied systematically to investigate the effect of epitaxial mismatch. The Ni-Ni interactions in the cluster were modeled with a well-established embedded atom model (EAM) potential,[25,26] and the pairwise Ni-C binding was approximated using the Lennard-Jones potential $V(r) = 4\varepsilon[(\sigma/r)^{12} - (\sigma/r)^6]$, smoothly truncated at 12 Å. The well depth ε was systematically varied to control substrate wettability, which we characterize in terms of the liquid-particle contact angle θ_l. Figure 2 illustrates that by adjusting ε one can precisely specify a desired θ_l. Note that the experimentally measured[22] $\theta_l \sim 50^\circ$ corresponds to $\varepsilon \approx 60$ meV. The value of σ was fixed at 2.8 Å, which was determined using an arithmetic mixing rule: $\sigma_{\text{Ni-C}} = (\sigma_{\text{Ni}} + \sigma_{\text{C}})/2$; where $\sigma_{\text{Ni}} = 2.22$ Å (Ref. 27) and $\sigma_{\text{C}} = 3.407$ Å.[28] In this study, however, we are less concerned about the accuracy of these parameters for the Ni-C interactions than in assessing the difference between an atomistic substrate and the structureless, mean-field surface used previously.[14,15,29] Although both approaches are very simple, the advantage of using an atomistic surface is that it allows one to adjust the microscopic structure of the substrate and study the effects of epitaxial strain.

We consider only closed-shell Ni icosahedra consisting of 147, 309, 561, 923, 1415, 2057 and 2869 atoms. These structures are the ground-state configurations under this potential in the absence of a substrate.[30] They were initially placed within a distance of $\sim 2\sigma$ from the fixed graphene sheet and then relaxed at a temperature $\sim$200 K below the corresponding melting point for a range of ε values. They were then gradually heated in increments of 10 K, allowing the system to first equilibrate for 0.5 to 1.0 ns and then evolve for another 0.5 ns to generate statistical averages.

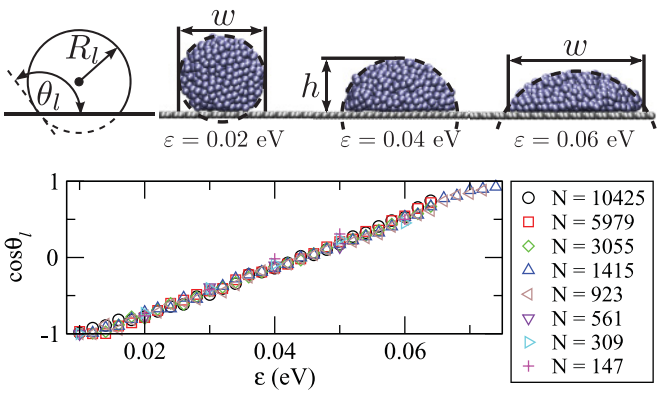

FIG. 2. (Color online) An illustration of how ε affects the geometry of molten Ni clusters on graphene. We extracted (time-averaged) w and h from our simulations and then computed the contact angle (θ_l) and the curvature radius (R_l) using the geometry of spherical caps: $R_l = \tilde{w} \equiv w/2$ if $\tilde{w} \geqslant h$ or $R_l = h(1 + \tilde{w}^2 h^{-2})/2$ if $\tilde{w} < h$; $\cos\theta_l = 1 - hR_l^{-1}$. The plot shows that $\cos\theta_l \propto \varepsilon$ for all Ni_N clusters considered here, and the trend is independent of cluster size N.

B. Order parameters

To characterize the melting transition we adopted the Steinhardt $\bar{q}_6$ order parameter[31] averaged using the scheme of Lechner and Dellago.[32] This order parameter relies on spherical harmonics, namely, $Y_{lm}(\mathbf{r}_{ij})$, to characterize angular symmetry in the arrangement of near neighbors j around each atom i. It is constructed by first defining $q_{lm}(i) = 1/N_b(i) \sum_j^{N_b(i)} Y_{lm}(\mathbf{r}_{ij})$, where $N_b(i)$ is the total number of near neighbors around atom i, then evaluating the arithmetic average of $q_{lm}(i)$ over all neighbors of i plus the atom i itself to obtain $\bar{q}_{lm}(i)$, and finally computing $\bar{q}_l(i) = \sqrt{(4\pi)/(2l+1) \sum_{m=-l}^{m=+l} |\bar{q}_{lm}(i)|^2}$. Setting $l = 6$ yields $\bar{q}_6(i)$, whose value is highly sensitive to local order around atom i. As in prior studies with Lennard-Jones systems,[32] we find that Ni atoms with symmetrically arranged neighbors (i.e., crystalline systems) yield $\bar{q}_6 > 0.35$ and disordered atoms (i.e., liquid systems) yield $\bar{q}_6 < 0.31$. Thus, atoms with $\bar{q}_6 < 0.33$ at any time t were defined as "liquid" at that t. However, this scheme is sensitive to the local order in a liquid and can slightly exaggerate the number of "solid" atoms. To avoid underestimating the liquid fraction ϕ_L, those atoms that were liquid on average (i.e. $\langle \bar{q}_6 \rangle_t < 0.33$) were so classified for all t. The melting temperature was then consistently defined by the point when the equilibrium liquid fraction $\langle \phi_L \rangle$ (an average of 100 instantaneous values) first reaches 0.9. We refrained from using $\langle \phi_L \rangle = 1$ as our threshold to compensate for the ordering of liquid atoms near the substrate.

To characterize the structure of solid Ni clusters we used common-neighbor analysis (CNA),[33,34] where each pair of nearest neighbors is assigned a set of four (Honeycutt) indices that uniquely identify a possible local symmetry. The local environment of an atom can then be inferred from the set of all

associated indices, with each member of that set corresponding to a "bond" with a particular near neighbor. Here we use CNA signatures listed by Hendy and Doye[35] to identify atoms with fcc, hcp, and icosahedral (ico) local order.

III. RESULTS AND DISCUSSION

Before considering the melting transition, the central issue of this work, we first discuss in Sec. III A the equilibrium structures of graphene-supported Ni clusters prior to complete melting. The aim is to illustrate how substrate binding strength and crystal structure can alter the morphology of solid metal clusters. In Sec. III B we investigate the influence of substrates on the melting transition. We first consider how substrate binding strength affects the melting temperature of Ni clusters on epitaxially matched graphene; and then we systematically vary the substrate lattice constant to induce epitaxial strain and demonstrate its ramifications on the melting transition. Finally, in Sec. III C we interpret the effects of induced epitaxial strain on the melting temperature using a prior phenomenological model.[17]

A. Substrate-induced solid-solid transition

When the initial closed-shell Ni icosahedra were relaxed on graphene with different ε, we found that $\varepsilon \geqslant 25$ meV led to a reconstruction into lamellar-twinned fcc particles. This transition can be identified by a small step in the caloric curves below T_m and, as we show for Ni_{1415} in Fig. 3, it leads to

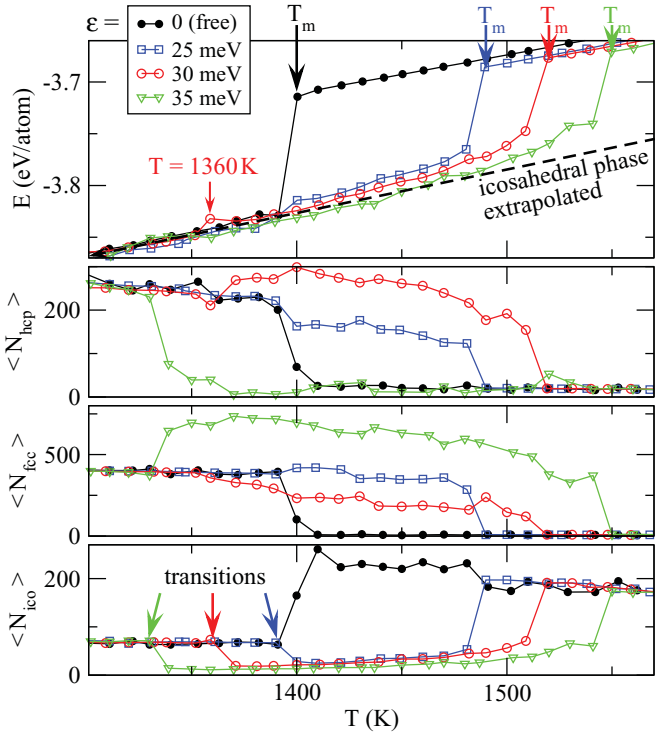

FIG. 3. (Color online) The internal energy E and the time-averaged number of hcp (N_{hcp}), fcc (N_{fcc}), and ico (N_{ico}) atoms are plotted versus temperature for Ni_{1415} on graphene with different ε values. Solid-solid transitions lead to a drop in $\langle N_{ico}\rangle$ correlating with an increase in $\langle N_{fcc}\rangle$ or $\langle N_{hcp}\rangle$, and they occur near the melting temperature T_m of unsupported Ni_{1415}.

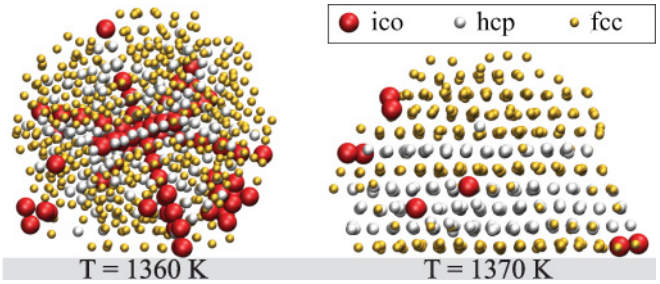

FIG. 4. (Color online) Snapshots of graphene-supported Ni_{1415} ($\varepsilon = 0.03$ eV) illustrating the icosahedral fivefold symmetry axes (ico atoms are large red spheres) vanishing between 1360 and 1370 K. The substrate is depicted in gray with the constituent atoms not shown.

a drop in the number of atoms with icosahedral symmetry (N_{ico}). Note that the local symmetry was characterized using CNA and the number of atoms with fcc (N_{fcc}), hcp (N_{hcp}), and icosahedral local order was averaged over time. Figure 3 also shows that the drop in N_{ico} correlates with a slight increase in N_{fcc} or N_{hcp}, and in Fig. 4 we further illustrate that this corresponds to the destruction of the icosahedral fivefold symmetry axes. Solid-solid transitions of this sort, namely, from noncrystalline structures such as icosahedra and decahedra to crystalline fcc, have been observed in experiments with Au clusters on amorphous carbon[36] and Ag clusters on Si(001) surfaces.[37,38] Although such solid-solid transitions have also been demonstrated using molecular dynamics simulations of unsupported clusters,[39,40] here we find that free (i.e., $\varepsilon = 0$) Ni clusters retain icosahedral symmetry right up until the melting point, and the transition to the lamellar-twinned fcc phase occurs only when the substrate binding strength exceeds some finite value (namely, $\varepsilon \geqslant 25$ meV). Hence, as was found in our previous study of a Pd_{887} decahedron on graphene,[41] the solid-solid transition here is clearly driven by substrate effects.

An interesting feature of Fig. 3 is that, for weak cluster-substrate interactions ($25 \leqslant \varepsilon < 35$ meV), the solid-solid transition leads to a slight *increase* in internal energy E, suggesting that entropic effects play an important role.[42] For strong cluster-substrate interaction ($\varepsilon \geqslant 35$ eV), however, the transformation is followed by a decrease in internal energy, indicating that closed-shell icosahedra cease to be the ground-state configuration. In all the cases considered here, we find that the mechanism via which the transition occurs is that illustrated in Fig. 5, corresponding to almost complete melting of the initial icosahedra followed by their recrystallization into a lamellar-twinned fcc particle. This mechanism has been discussed in prior work,[36,41,43,44] and it is attributed to the high free-energy barrier associated with the breaking of closed-shell clusters when "wetting" a substrate.

It is also worth noting that in all of our simulations with graphene as the supporting surface, the adjacent nickel atoms always form a close-packed (111) surface once a cluster is relaxed. However, it is reasonable to expect that substrates with other crystal structures could lead to different facet formations. For instance, Li and Zuo[37] found that their fcc Ag clusters formed (001) facets that epitaxially matched the underlying Si(001) surface. Similar contact epitaxy was also observed in simulations of Cu, Ag, Au, Pt, and Ni clusters on (100) surfaces of matching material.[44] To explore this

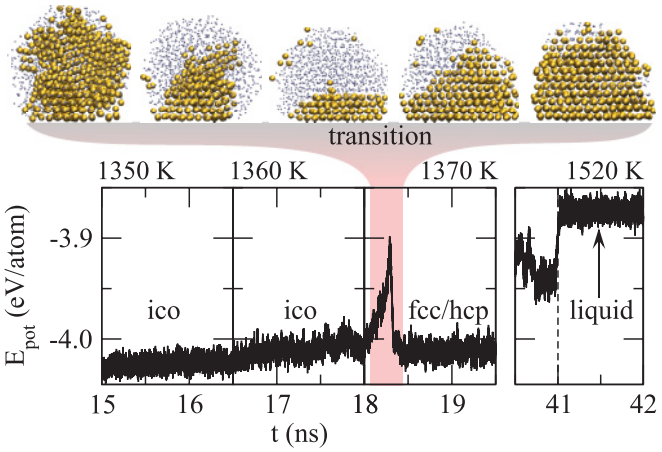

FIG. 5. (Color online) Time evolution of the potential energy $E_{\rm pot}$ of Ni_{1415} on graphene with $\varepsilon = 0.03$ eV at different temperatures. The spike in $E_{\rm pot}$ at 1370 K corresponds to the icosahedral structure melting almost entirely and then recrystallizing into an fcc and hcp arrangement. The sequence of cluster snapshots illustrate this process, with larger golden spheres representing the solid Ni atoms and smaller blue dots representing the liquid Ni atoms. Substrate atoms not shown.

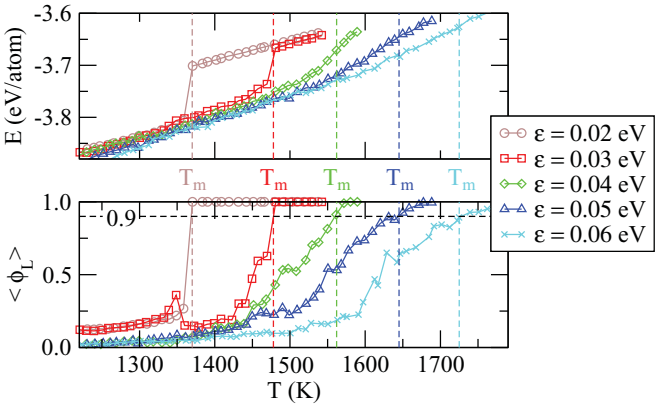

FIG. 6. (Color online) A sample from the simulated data that was used to characterize the melting transition in supported Ni_{923} for different substrate binding strengths (ε). A steep rise in the equilibrium liquid fraction $\langle\phi_L\rangle$ correlates with the absorption of latent heat in the corresponding caloric curves. Each melting temperature (T_m) is defined by the point when $\langle\phi_L\rangle = 0.9$.

further, we ran simulations of Ni_{923} on a single layer of carbon atoms arranged in a cubic lattice. The value of ε was fixed at 0.03 eV and we varied the substrate lattice spacing (s) to stimulate the formation of a Ni(100) facet. We were successful in doing so for s between 2.4 and 2.5 Å, which closely matches the equilibrium Ni-Ni separation (2.49 Å); whereas specifying s outside this range led to the formation of close-packed Ni(111) facets. This demonstrates the possibility of controlling the orientation of crystal planes in supported nanoparticles by selecting appropriate substrates, which could be exploited in catalytic applications such as the growth of carbon nanotubes,[5,45] and it suggests that using mean-field substrates without atomic roughness[14,15,29] may not be sufficient for correctly predicting the phase of supported nanoparticles.

B. Substrate effects on the melting temperature

Having analyzed the structure of graphene-supported solid nickel clusters at elevated temperatures, we now consider their melting. The solid-liquid phase transition can usually be identified by a sudden increase in internal energy (E) due to the absorption of latent heat. Figure 6 shows some of the simulated caloric data where the melting of supported Ni_{923} is apparent, and the absorption of latent heat correlates with an increase in the equilibrium liquid fraction $\langle\phi_L\rangle$—our order parameter. Interestingly, the phase transition changes from being abrupt to gradual as ε increases. The broadening persists in simulations with slower heating rates, indicating that it is not due to an increase in relaxation times, and later we will show that it can be attributed to surface melting. Similar broadening was exhibited by all other Ni clusters considered here, leading to some ambiguity into where exactly the melting occurs, which is why we resorted to using the order parameter $\langle\phi_L\rangle$ to consistently define T_m. Note that the bump in $\langle\phi_L\rangle$ at $T \approx 1350$ K for $\varepsilon = 0.03$ eV is due to the transition from icosahedral to fcc order as discussed in Sec. III A.

From the simulations with different ε, where Ni and graphene are epitaxially matched and strain effects are negligible, we can deduce the response of T_m to changes in R_l. The resultant trends in $T_m(R_l)$ are shown in Fig. 7, together with the data for free icosahedra and decahedra of different sizes. It is evident that, contrary to what was found in prior studies,[14,16] Ni clusters supported on graphene do not follow the same trend as the unsupported structures. Rather we find that the melting temperature of supported clusters is consistently higher than that of the closed-shell icosahedra and decahedra with the same radius of curvature. This trend suggests that the atomistic graphene sheet stabilizes the crystalline phase of Ni clusters in a way that mean-field substrates[14,15] do not.

To ascertain if favorable epitaxy is the cause for the apparent stabilization, we now induce epitaxial strain in supported Ni_{923} by isotropic scaling of the substrate lattice constant a while keeping ε fixed. Such scaling specifies the in-plane substrate strain $\delta \equiv (a - a_0)/a_0$, where $a_0 = 2.5$ Å. It also alters the net substrate binding and, hence, the curvature of the clusters' free surface. The obtained $T_m(R_l)$ data [see Fig. 8(a)] initially follow the strain-free trend, but then approach that of unsupported clusters as R_l increases. Such behavior is due to both epitaxial strain and changes in the curvature of the free surface of the particle. To correct for curvature variation we can subtract from each data point the value of $T_m(R_l)$ computed using Eq. (1) with T_c and $\mathcal{C}$ fitted to the strain-free data. In Fig. 8(a) this corresponds to subtracting from each green square and blue diamond the value of the red dashed curve at the same R_l, giving an estimate of the deviation ΔT_m [plotted in Fig. 8(b)] that results from induced epitaxial strain.

Figure 8(b) shows that δ, irrespective of its sign, depresses the melting temperature of a cluster with a given R_l. This happens because stretching or compressing graphene along the plane ruins its epitaxial alignment with the adjacent Ni(111) surface and destabilizes the solid phase. Note that Ni atoms at the cluster-substrate interface can arrange themselves in many different ways in response to epitaxial strain; hence the induced strain in supported particles may not exactly correspond to the

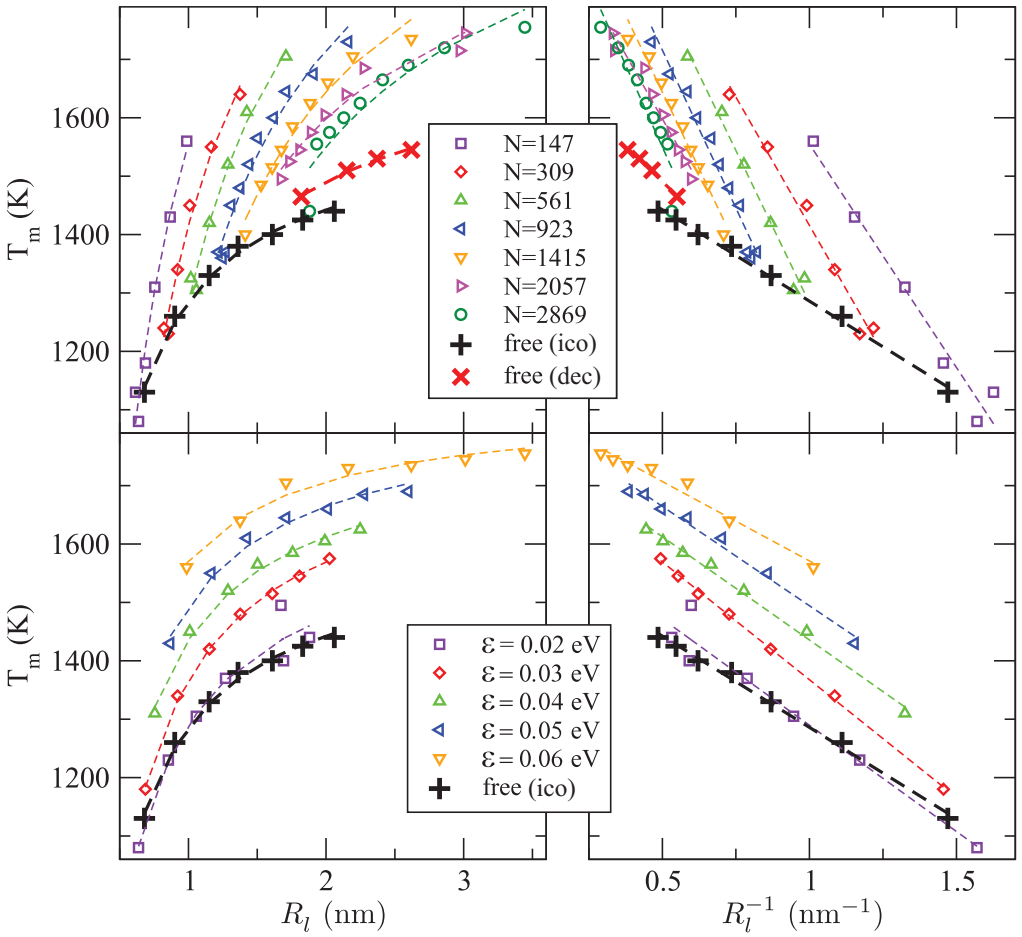

FIG. 7. (Color online) The melting temperature of graphene-supported Ni clusters versus the curvature (R_l^{-1}) of the free surface. Unsupported closed-shell icosahedra and decahedra—the lowest-energy structures for this size range in the absence of a substrate—are also included for comparison. All four panels show exactly the same data for supported clusters, but sorted differently. In the top panels the data are divided into subsets with the same number of constituent atoms (N), and the trends illustrate how T_m changes when R_l is altered through variation in ε. In the bottom panels the data sets are sorted by the specified ε, demonstrating changes in T_m when R_l is altered through variation in N (ε constant). Panels on the right show that in both cases the subsets roughly follow $T_m \propto R_l^{-1}$. Dashed curves show Eq. (1), with both T_m and $\mathcal{C}$ fitted, and serve merely as a guide to the eye.

specified δ, possibly accounting for the relatively larger scatter of ΔT_m values around the general trend. Also note that some of the data points mark the melting temperature of closed-shell icosahedra, while the rest correspond to lamellar-twined fcc particles. In spite of these apparent incongruities, there is a clear concave-down trend centered at zero strain, and its width diminishes as ε increases. The trend narrows because increasing ε leads to a larger cluster-substrate interfacial area, making the solid Ni_{923} more sensitive to epitaxial effects. It is worth mentioning that the concave-down trend is similar to the quadratic depression of the bulk melting temperature in strained surfaces.[46] Here, however, the depression is not with respect to the bulk melting temperature T_c, but to the value $T_m(R_l)$ that is already reduced by curvature effects.

C. Comparison with phenomenology

To reconcile the epitaxial strain-induced ΔT_m observed in our simulations with Eq. (2), we show in Fig. 9 that there is indeed a noticeable change in curvature radius (R) and contact angle (θ) during the melting simulations. Note that both R and θ are ill defined for solid nanoparticles with pronounced faceting, but when the free surface of nanoparticles roughens, just below the melting transition, then both quantities can be defined unambiguously. As melting initiates, and as the liquid fraction increases, we find that R decreases (i.e., $R_s > R_l$) and θ increases (i.e., $\theta_s < \theta_l$). This noticeable reduction in wetting supports our argument that the underlying substrate has a stronger affinity for a surface-roughened crystal than for a liquid droplet. An increase in θ of similar magnitude was also detected on strained graphene, implying that substrates considered here never favor the liquid phase, which is partially an artifact due to the symmetry and planar arrangement imposed on substrate atoms. This observation is consistent with Fig. 8(a) (and Fig. 7), where all of the supported clusters are shown to have a higher T_m than unsupported structures of comparable curvature—even when the substrate is strained.

Phenomenologically, for an epitaxially matched substrate the solid-cluster–substrate interface energy is relatively low,

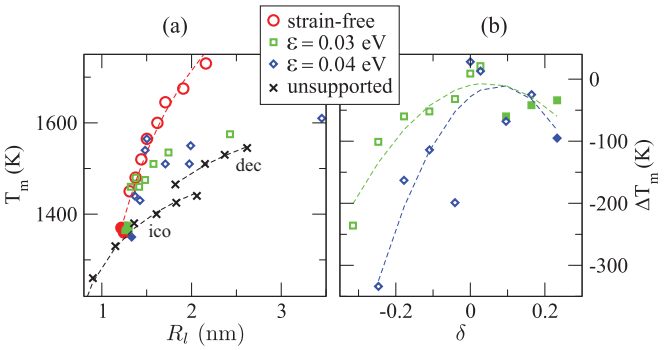

FIG. 8. (Color online) (a) Melting temperatures (T_m) of supported Ni_{923} clusters as a function of curvature radius of the liquid phase (R_l). In the approximately strain-free data (red circles), the graphene lattice spacing was fixed while ε was varied. For the specified ε values, namely, $\varepsilon = 0.03$ and 0.04 eV, the data points were obtained by straining the substrate (i.e., changing δ from about -0.3 to 0.2). T_m values for unsupported icosahedral (ico) and decahedral (dec) clusters of different sizes are included for comparison. Dashed curves correspond to Eq. (1) with both T_c and $\mathcal{C}$ fitted. (b) Strain-induced shifts in melting temperature (ΔT_m) of Ni_{923} as a function of specified substrate strain δ. Each ΔT_m was calculated by taking T_m of Ni_{923} on substrates with specified δ and then subtracting the value of the strain-free $T_m(R_l)$ trend at the corresponding R_l. Dashed curves are quadratic fits and serve as a guide to the eye. Note that filled symbols correspond to clusters that remained icosahedral until the melting transition, while unfilled symbols correspond to clusters that were in the lamellar-twinned fcc phase.

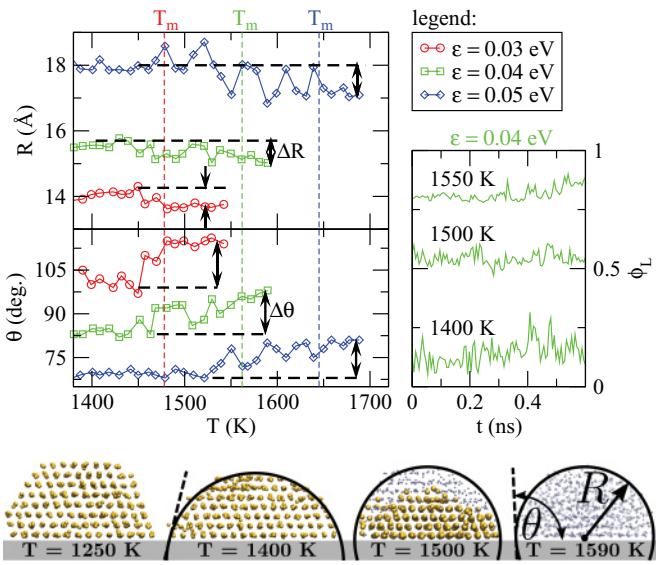

FIG. 9. (Color online) The radius of curvature (R) and contact angle (θ) are shown to increase ($\Delta\theta \sim 15^\circ$) as the liquid fraction grows during the melting of Ni_{923} on graphene (with minimal epitaxial strain). Evolution of the instantaneous liquid fraction (ϕ_L) indicates a broad temperature range over which large liquid fractions remain stable (for 0.6 ns). Snapshots illustrate the atomic structure of Ni_{923} with $\varepsilon = 0.04$ eV at different temperatures, with each atom classified as either "solid" (gold spheres) or "liquid" (blue dots) using the Steinhardt $\bar{q}_6$ parameter (see Sec. II B).

while introduction of epitaxial strain effectively raises that energy and leads to a decrease in R_s.[17] Since liquids are inherently more disordered, the value of R_l is not expected to decrease by as much, and from (2) we see that this should cause T_m to drop. Extracting $R_s^{-1} - R_l^{-1} \approx -0.03$ nm^{-1} from Fig. 9 and using $T_c \approx 1740$ K,[26] $L \approx 0.18$ eV/atom,[26] $\rho \approx 80$ atoms/nm^3,[47] and $\gamma_l \approx 10$ eV/nm^2,[48] we obtain $\Delta T_m \sim 100$ K, which is an order-of-magnitude estimate of the discrepancy between (1) and (2). This discrepancy is entirely due to the failure of (1) to account for substrate-induced epitaxial strain, and it is of the same order of magnitude as the ΔT_m obtained from molecular dynamics simulations in Fig. 8(b). More importantly, both quantities are comparable to the melting point depression due to curvature alone, indicating that substrate effects can be just as significant as size effects. In fact, simulations of Ni_{2057} and Ni_{2869} on strain-free graphene resulted in slight superheating (see Fig. 7), yielding respective melting temperatures of 1745 and 1755 K for $\varepsilon = 0.06$ eV. (Note that the EAM potential used here yields $T_m = 1740$ K for bulk Ni.[26]) However, unlike confined thin films[20] and nanoparticles embedded in matrices,[21] confinement and pressure-induced effects do not play a role here. Hence, the overheating we report is primarily due to favorable epitaxy.

Another noteworthy feature in Fig. 9 is the stability of large liquid fractions. For $\varepsilon = 0.04$ eV, the melting temperature of strain-free Ni_{923} is estimated to be 1560 K. At 1550 K, however, ϕ_L fluctuates about a well-defined mean value of $\sim$0.8 throughout the entire simulation. From the steady nature and magnitude of these fluctuations we infer that the broadening of the melting transition is due to the onset of surface melting,[49,50] as opposed to dynamic coexistence where the cluster oscillates between fully liquid and fully solid states.[30] Cluster snapshots support this deduction: the liquid always nucleates near the free surface and gradually progresses inward as the temperature rises. It is interesting that the strongly adhered nanoparticles studied here appear to melt entirely in a continuous fashion, which was not observed in simulations with mean-field substrates,[14,15] indicating that epitaxial effects arising from atomistic substrates can help stabilize surface-melted nanoparticles.

IV. SUMMARY

To summarize, we have used molecular dynamics simulations to demonstrate that favorable epitaxy can raise the melting temperature of supported nanoparticles by hundreds of degrees. Such an enhancement of the melting temperature is important, because catalytic activity can be strongly influenced by the surface structure of a nanoparticle: a substrate that enhanced the melting temperature of a supported catalyst particle would allow operation at higher temperatures than would otherwise be the case, potentially giving access to new catalytic pathways and reactions. Furthermore, the magnitude of this effect was shown to be in quantitative agreement with a thermodynamic model[17] (2), suggesting that it can be modeled phenomenologically. Our simulations also indicate that strongly binding, epitaxially matched substrates can stabilize surface-melted nanoparticles, causing significant broadening of the melting transition, and can induce solid-solid transitions at elevated temperatures. These findings suggest

that substrates may be used to controllably tune the melting and premelting behavior of supported nanoparticles through epitaxy, and they motivate more comprehensive studies of the effects of substrate-induced epitaxial strain on the equilibrium phase of nanostructures.

ACKNOWLEDGMENTS

We thank the Royal Society of New Zealand for funding through Marsden Fund Contract No. IRL0602, and the MacDiarmid Institute for Advanced Materials and Nanotechnology for computational facilities.

[1] P. Pawlow, Z. Phys. Chem. **65**, 1 (1909).
[2] F. Baletto and R. Ferrando, Rev. Mod. Phys. **77**, 371 (2005).
[3] K. Nanda, Pramana **72**, 617 (2009).
[4] A. S. Barnard, Rep. Prog. Phys. **73**, 086502 (2010).
[5] M. H. Kuang, Z. L. Wang, X. D. Bai, J. D. Guo, and E. G. Wang, Appl. Phys. Lett. **76**, 1255 (2000).
[6] S. Helveg, C. López-Cartes, J. Sehested, P. Hansen, B. Clausen, J. Rostrup-Nielsen, F. Abild-Pedersen, and J. Nørskov, Nature (London) **427**, 426 (2004).
[7] S. Hofmann, R. Sharma, C. Ducati, G. Du, C. Mattevi, C. Cepek, M. Cantoro, S. Pisana, A. Parvez, F. Cervantes-Sodi *et al.*, Nano Lett. **7**, 602 (2007).
[8] J. G. Partridge, S. A. Brown, A. D. F. Dunbar, R. Reichel, M. Kaufmann, C. Siegert, S. Scott, and R. J. Blaikie, Nanotechnology **15**, 1382 (2004).
[9] C. Thelander, M. H. Magnusson, K. Deppert, L. Samuelson, P. R. Poulsen, J. Nygard, and J. Borggreen, Appl. Phys. Lett. **79**, 2106 (2001).
[10] P. Buffat and J.-P. Borel, Phys. Rev. A **13**, 2287 (1976).
[11] K. F. Peters, J. B. Cohen, and Y.-W. Chung, Phys. Rev. B **57**, 13430 (1998).
[12] M. Zhang, M. Y. Efremov, F. Schiettekatte, E. A. Olson, A. T. Kwan, S. L. Lai, T. Wisleder, J. E. Greene, and L. H. Allen, Phys. Rev. B **62**, 10548 (2000).
[13] C. Mottet and J. Goniakowski, Surf. Sci. **566–568**, 443 (2004).
[14] F. Ding, A. Rosén, S. Curtarolo, and K. Bolton, Appl. Phys. Lett. **88**, 133110 (2006).
[15] Y. Shibuta and T. Suzuki, Phys. Chem. Chem. Phys. **12**, 731 (2010).
[16] A. Jiang, N. Awasthi, A. N. Kolmogorov, W. Setyawan, A. Börjesson, K. Bolton, A. R. Harutyunyan, and S. Curtarolo, Phys. Rev. B **75**, 205426 (2007).
[17] S. C. Hendy, Nanotechnology **18**, 175703 (2007). Note that there is a typo in Eq. 5: the + sign should be a −.
[18] E. Z. Luo, Q. Cai, W. F. Chung, and M. S. Altman, Appl. Surf. Sci. **92**, 331 (1996).
[19] T. Schülli, R. Daudin, G. Renaud, A. Vaysset, O. Geaymond, and A. Pasturel, Nature (London) **464**, 1174 (2010).
[20] L. Zhang, Z. H. Jin, L. H. Zhang, M. L. Sui, and K. Lu, Phys. Rev. Lett. **85**, 1484 (2000).
[21] H. Sheng, G. Ren, L. Peng, Z. Hu, and K. Lu, J. Mater. Res. **12**, 119 (1997).
[22] Y. V. Naidich, V. M. Perevertailo, and G. M. Nevodnik, Powder Metall. Met. Ceram. **10**, 45 (1971).
[23] S. Plimpton, J. Comput. Phys. **117**, 1 (1995).
[24] M. G. Paterlini and D. M. Ferguson, Chem. Phys. **236**, 243 (1998).
[25] S. M. Foiles, M. I. Baskes, and M. S. Daw, Phys. Rev. B **33**, 7983 (1986).
[26] S. M. Foiles and J. B. Adams, Phys. Rev. B **40**, 5909 (1989).
[27] P. M. Agrawal, B. M. Rice, and D. L. Thompson, Surf. Sci. **515**, 21 (2002).
[28] J. P. Lu, X.-P. Li, and R. M. Martin, Phys. Rev. Lett. **68**, 1551 (1992).
[29] U. Sarkar and S. A. Blundell, Phys. Rev. B **79**, 125441 (2009).
[30] D. Schebarchov and S. C. Hendy, J. Chem. Phys. **123**, 104701 (2005).
[31] P. J. Steinhardt, D. R. Nelson, and M. Ronchetti, Phys. Rev. B **28**, 784 (1983).
[32] W. Lechner and C. Dellago, J. Chem. Phys. **129**, 114707 (2008).
[33] J. Honeycutt and H. Andersen, J. Phys. Chem. **91**, 4950 (1987).
[34] D. Faken and H. Jónsson, Comput. Mater. Sci. **2**, 279 (1994).
[35] S. C. Hendy and J. P. K. Doye, Phys. Rev. B **66**, 235402 (2002).
[36] K. Koga, T. Ikeshoji, and K.-i. Sugawara, Phys. Rev. Lett. **92**, 115507 (2004).
[37] B. Q. Li and J. M. Zuo, Phys. Rev. B **72**, 085434 (2005).
[38] K. Sato, W. J. Huang, F. Bohra, S. Sivaramakrishnan, A. P. Tedjasaputra, and J. M. Zuo, Phys. Rev. B **76**, 144113 (2007).
[39] D. Schebarchov and S. C. Hendy, Eur. Phys. J. D **43**, 11 (2007).
[40] T. T. Järvi, A. Kuronen, K. Nordlund, and K. Albe, J. Appl. Phys. **102**, 124304 (2007).
[41] D. Schebarchov, S. C. Hendy, and W. Polak, J. Phys.: Condens. Matter **21**, 144204 (2009).
[42] J. P. K. Doye and F. Calvo, Phys. Rev. Lett. **86**, 3570 (2001).
[43] K. Shintani, Y. Taniguchi, and S. Kameoka, J. Appl. Phys. **95**, 8207 (2004).
[44] T. T. Järvi, A. Kuronen, K. Meinander, K. Nordlund, and K. Albe, Phys. Rev. B **75**, 115422 (2007).
[45] N. Ishigami, H. Ago, K. Imamoto, M. Tsuji, K. Iakoubovskii, and N. Minami, J. Am. Chem. Soc. **130**, 9918 (2008).
[46] U. Tartaglino and E. Tosatti, Surf. Sci. **532–535**, 623 (2003).
[47] F. J. Cherne, M. I. Baskes, and P. A. Deymier, Phys. Rev. B **65**, 024209 (2001).
[48] M. Chen, C. Yang, and Z.-Y. Guo, Mater. Sci. Eng. A **292**, 203 (2000).
[49] J. W. M. Frenken and J. F. van der Veen, Phys. Rev. Lett. **54**, 134 (1985).
[50] H. Sakai, Surf. Sci. **351**, 285 (1996).